Development of solid polymer electrolytes based on poly(vinylidene fluoride-trifluoroethylene) and the $[N_1 1_1 1_2(OH)][NTf_2]$ ionic liquid for energy storage applications

R. Leones [a,d], C.M. Costa [b], A.V. Machado [c], J.M.S.S. Esperança [d], M.M. Silva [a], S. Lanceros-Méndez [b,*]

[a] Centro/Departamento de Química, Universidade do Minho, 4710-057 Braga, Portugal

[b] Centro/Departamento de Física, Universidade do Minho, 4710-057 Braga, Portugal

[c] IPC - Institute for Polymers and Composites, Universidade do Minho, Campus de Azurém, 4800-058 Guimarães, Portugal

[d] Instituto de Tecnologia Química e Biológica, Universidade Nova de Lisboa, 2780-157 Oeiras, Portugal

Keywords:

Membranes
Ionic liquid
P(VDF-TrFE)
Energy storage

Abstract

P (VDF-TrFE), solid polymer electrolytes were prepared using the ionic liquid N,N,N-trimethyl-N-(2-hydroxyethyl) ammonium bis(trifluoromethylsulfonyl)imide, $[N_1112(OH)][NTf_2]$. The morphology, polymer phase, and thermal and electrochemical properties have been determined by scanning electron microscopy (SEM), Fourier Transform

Infrared Spectroscopy (FTIR), differential scanning calorimetry (DSC) and impedance spectroscopy, respectively. The addition of the ILs in P(VDF-TrFE) affects the microstructure, thermal stability and ionic conductivity of the polymer membrane. It was found that the ionic conductivity increases as the ionic liquid (IL) content increases with a maximum value at room temperature of $1.7 \times 10^{-5}\ \mathrm{S} \cdot \mathrm{cm}^{-1}$ for an IL composition of $32\mathrm{wt.\%}$. The temperature behavior in the ionic conductivity is thermally activated, following the Arrhenius equation, the high ionic conductivity resulting from the large carrier numbers of the IL. The electrochemical potential window shows 1.0 V at 4.0 V that these solid polymer electrolytes are adequate for energy storage devices.

Introduction

Solid-state ionic conductors, such as solid polymer electrolytes (SPEs) [1-3], have attracted considerable attention as components for commercial applications in particular rechargeable lithium batteries [1,4-6] and fuel cells [7,8]. The rechargeable lithium polymer battery is one of the most promising high energy storage devices [9]. A wide variety of SPEs mainly based on the ethylene oxide repeat unit have been synthesized and characterized, being at the basis of most commercially available SPEs [4]. The resulting macromolecules include linear and branched polymers, block copolymers and plasticized polymers as well as organic/inorganic hybrids, with morphologies that almost cover the entire range between amorphous and crystalline states [10-15]. Different polymers are being also evaluated as potential electrolyte materials for polymer batteries [16]. Among them, poly(vinylidene fluoride) (PVDF) and copolymers are particularly interesting [17] due to their semicrystallinity, chemical resistance, excellent mechanical strength, relatively high dielectric constants and high anodic stability due to the presence of strong electron-withdrawing function groups ($-\mathrm{C}-\mathrm{F}-$) [18-21]. Despite the enormous technological potential of solvent-free SPEs, they

suffer from a serious drawback: a relatively low ionic conductivity. The addition of ionic liquids (ILs) to SPEs appears as a possible solution due to the enhancement of the electrochemical stability and the ionic conductivity [22]. ILs are salts with melting points below $100\ ^{\circ}\mathrm{C}$ [23] that gained prominence for this application due to some important characteristics such as high ionic conductivity ($\sim 10^{-3} - 10^{-2}\ \mathrm{S} \cdot \mathrm{cm}^{-1}$) [24], almost null volatility [25], null flammability [26], thermal stability [27], wide electrochemical windows ($\sim 4 - 6\ \mathrm{V}$) [28], environment-friendly and the interchangeability between the many different possible cations and anions that can be used in a tunable fashion [29] in comparison to the conventional liquid electrolyte (salts dissolved in organic solvent). Several problems in the use of ILs arise from their high viscosity and low mobility of the ions [30]. Changes in both cation and/or anion of the IL allow tuning their characteristics, such as density, viscosity, electrical conductivity, and electrochemical stability [31-33]. ILs have two important features for their specific use in battery applications: very high concentrations of ions and high ion mobility at room temperature. Since many ILs show ionic conductivities of $10^{-2}\ \mathrm{S} \cdot \mathrm{cm}^{-1}$ or above at room temperature, there are many possible applications as electrolyte materials [31], for high concentration of ILs being able to eliminate the electrolyte depletion problems encountered in conventional liquid electrolytes. The majority of ILs are compatible with the solvents present in the most used electrolyte solution, also improving the mechanical properties of the polymer matrix [34]. The use of PVDF polymer and ILs as SPEs is almost unexplored. The most used co-polymer of PVDF for SPEs is poly(vinylidene fluoride)-co-hexafluoropropylene, PVDF-HFP [35-37]. For rechargeable magnesium batteries, the

magnesium triflate salt, $Mg(Tf)_2$, has been used, within an ionic liquid, 1-ethyl-3methylimidazolium trifluoro-methanesulfonate (EMITf). This solution is then placed in poly(vinylidene fluoride-hexafluoropropylene) (PVDF-HFP). The system shows high ionic conductivity at room temperature, $\sim 4.8 mS \cdot cm^{-1}$ and excellent thermal and electrochemical stabilities [38].

This work investigates the thermal and electrochemical properties of electrolytes prepared through the addition of controlled quantities of the ionic liquid N,N,N-trimethyl-N-(2-hydroxyethyl)ammonium bis(trifluoromethylsulfonyl)imide, $[N_1112(OH)][NTf_2]$ to poly(vinylidene fluoride-co-trifluoroethylene), P(VDF-TrFE), host networks, prepared by solvent casting. The choice of $P(VDF-TrFE)$ is due to its high dipolar moment, high dielectric constant ($\varepsilon \sim 12$), possibility of controlling its pore size and degree of porosity at room temperature, its low degree of crystallinity and good mechanical properties. For specific molar ratios of VDF and TrFE (example: 70/30) the polymer crystallizes, both from the melt and by solution casting, in a highly polar ferroelectric transplanar chain configuration, TT, similar to the one of the β-phase of PVDF [17,39,40]. Current trends in ionic liquids research tend to use more eco-friendly ionic liquids, such as the ionic liquid $[N_1 \ 1 \ 1 \ 2(OH)] [NTf_2]$. Further, this IL shows high thermal stability and adequate thermo-physical properties for the application under consideration [33]. The ionic conductivity and electrochemical stability were determined and related to the morphology variation at a molecular level of the electrolyte.

Experimental

Membrane preparation

Poly(vinylidene fluoride-trifluoroethylene) (P(VDF-TrFE), (monomer mole ratio = $70/30), M_w = 350000$ g/mol, Solvay) was dissolved in tetrahydrofuran (THF) (Acros Organics, 99.9%) in a proportion of 10/90 at room temperature and under magnetic stirring for a few minutes. To this solution were added different quantities of ionic liquid N,N,N-trimethyl-N-(2-hydroxyethyl)ammonium bis(trifluoromethylsulfonyl) imide, $[N_1112(OH)][NTf_2]$ (synthesized as described in [33], >99% with viscosity of 100 cP) ranging the relative ionic liquid/polymer concentration from 0 up to 32%(w/w). Finally, the solution was poured in a glass Petri dish and the THF solvent evaporated at room temperature.

Characterization

The obtained electrolyte membranes were coated with a thin gold layer using a sputter coating (Polaron, model SC502 sputter coater) and their morphology was analyzed using a scanning electron microscopy (SEM) (Cambridge, Leica) with an accelerating voltage of 15 kV .

The samples analyzed in cross-section were mechanically broken after immersing in liquid nitrogen for 180 s in order to ensure that the sample temperature decreases below glass transition (Tg).

The polymer phase of the membranes and possible interaction between the IL and the polymer matrix were determined by Fourier Transform Infrared Spectroscopy (FTIR) performed at room temperature with a PerkinElmer Spectrum 100 apparatus in ATR

mode from 4000 to 650 cm^{-1}. FTIR spectra were collected after 32 scans with a resolution of 4 cm^{-1}.

The thermal behavior of the membranes was evaluated by differential scanning calorimetry (DSC) between 25 and 200°C, at a heating rate of 10 $°C \cdot min^{-1}$, under a flowing argon atmosphere, using a Mettler DSC 821e. Measurements were performed in 40μ L aluminium cans with perforated lids.

The degree of crystallinity (χ_c) was calculated (Eq. (1)) from the enthalpy of the melting peak (ΔH_f), taking into consideration the enthalpy of fully crystalline PVDF ($\Delta H_{100} = 103.4$ J/g) [41]: $\chi_C = \frac{\Delta H_f}{\Delta H_{100}}$.

The ionic conductivity of the samples was determined by locating an electrolyte disk between two 10 mm diameter ion-blocking gold electrodes (Goodfellow, >99.95%) to form a symmetrical cell. The electrode/ polymer electrolyte/electrode assembly was secured in a suitable constant volume support and installed in a Buchi TO51 tube oven with a type K thermocouple placed close to the electrolyte disk to measure the sample temperature. Bulk conductivity of the electrolyte samples were obtained during heating cycles using the complex plane impedance technique (Autolab PGSTAT-12 (Eco Chemie)) between 15 and 100°C.

The ionic conductivity was calculated using Eq. (2):

$$\sigma = \frac{d}{R_b A} \tag{2}$$

where σ is the ionic conductivity, R_b is the bulk resistance, d is the thickness and A is the area of the sample.

The evaluation of the electrochemical stability of electrolytes was carried out under an argon atmosphere using a two-electrode cell configuration. The preparation of a 25μ m diameter gold microelectrode surface, by polishing with a moist cloth and 0.05μ m alumina powder (Buehler), was completed outside the drybox. The cell was assembled by locating a clean lithium disk counter electrode (19 mm diameter, 0.75 mm thick, Aldrich, 99.9% purity) on a stainless steel current collector and centering a electrolyte sample on the electrode surface. A small volume (2μ L) of THF was placed on the microelectrode surface. The microelectrode was then located on the electrolyte surface and supported firmly by means of a clamp. The use of THF to soften the electrolyte was necessary to achieve a reproducible microelectrode/electrolyte interfacial contact. An Autolab PGSTAT-12 (Eco Chemie) was used to record voltammograms at the 0,05; 0,1; 0,5 and 1 $V \cdot s^{-1}$ scanning rates. Measurements were performed at room temperature within a Faraday cage.

Results and discussion

Morphological properties and infrared characterization

Fig. 1a-d shows the SEM images of the SPE membranes with different IL contents: 0wt. %, 4wt. %, 16wt. % and 32wt. %, respectively.

The pristine $P(VDF-TrFE)$ membrane demonstrates the presence of uniformly distributed small pores approximately 5μ m in size as shown in Fig. 1a. The pore structure in the co-polymer has been explained by the phase diagram where a spinodal decomposition of the liquid-liquid phase separation and crystallization of the copolymer rich phase occurs [42]. This structure has also been observed for P(VDF-TrFE) dissolved in dimethylformamide, DMF [43]. The insert in Fig. 1a exhibits the dense spherulite morphology composing the material, with spherulite sizes of $\sim 1\mu$ m.

Fig. 1b-d shows the variations of the microstructure of the SPEs with increasing ionic liquid content, corresponding to an increase of the pore size from 9μ m to 30μ m and a decrease of the spherulite size. The reduction of the spherulite microstructure shown in Fig. 1d is correlated to the decreasing degree of crystallinity (Fig. 3, Table 1) with the addition of the ionic liquid.

Infrared spectroscopy was used to investigate the phase of the polymer and the possible interaction between the ionic liquid and host polymer.

The FTIR spectra of Fig. 2a show the pristine polymer and the SPEs with different ionic liquid contents in the region between 600 and 1600 cm^{-1}.

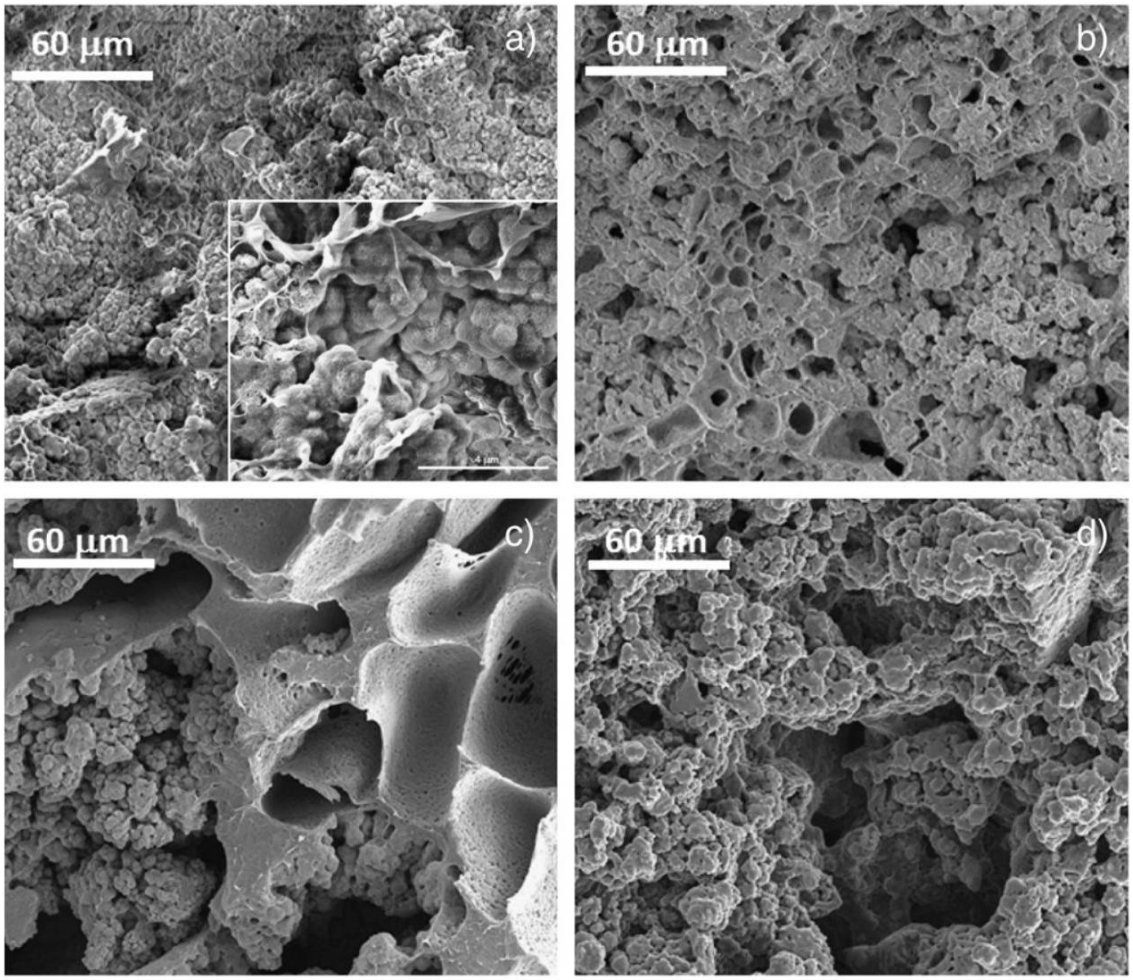

Fig. 1. Cross section SEM images of the P(VDF-TrFE) membranes with different IL contents: a) 0wt. %, b)4wt. %, c)16wt. % and d) 32wt. %.

The characteristic vibration modes at 851 cm^{-1}, 886 cm^{-1} and 1402 cm^{-1} [43], of the all-trans conformation of the polymeric matrix characteristic of the beta phase of the polymer is observed in all membranes, independently of the ionic liquid content. The presence of the ionic liquid does not influence the vibrational modes of the pristine polymer independently of its quantity.

The characteristics vibrational modes of the anion $[NTf_2]^-$at 1351 and 1061 cm^{-1} defined as the stretching vibration of $S = 0$ [44] are also observed. These vibrational modes increase as the ionic liquid content in the SPE membranes.

The FTIR region of the P (VDF-TrFE) polymer that represent the $C-H$ stretching vibrations [45] is shown in the Fig. 2b and can give information about the complexation of the inclusion of ILs in the polymer matrix.

In Fig. 2b two peaks are observed that represent the symmetric and asymmetric stretching vibrations of the CH_2 group at 2975 cm^{-1} ($\nu_s CH_2$) and 3013 cm^{-1} ($\nu_a CH_2$) in all membranes. It can be concluded the reduced interaction between an anion and a CH_2 group of P(VDFTrFE) polymer that depends of the anion size. Wang et al. showed that the

electrostatic interaction between the polymer chains and the ionic liquid becomes weaker for larger anions, resulting, for example, in a lower capability to induce the polar phases of PVDF [46].

Table 1

Melting temperature (T_m), Curie temperature (T_{FP}) and degree of crystallinity (χ_c) of the SPEs with different IL contents, as determined from the DSC scans.

Samples	$T_{FP}/°C \pm 2\%$	$T_m/°C \pm 2\%$	$\chi_c/\% \pm 2\%$
0wt. %	107	142	20
4wt. %	112	141	19
16wt. %	113	139	21
32wt. %	109	133	17

Thermal and electrical properties

Typical DSC scans of the SPEs with different ionic liquid contents are shown in Fig. 3 and their main characteristics such as melting temperature, T_m, ferroelectric-paraelectric phase transition - Curie temperature, T_{FP}, and degree of crystallinity, ΔX, are listed in Table 1.

The DSC scans of all the samples are characterized (Fig. 3) by two endothermic peaks in which the lower temperature peak corresponds to the ferroelectric-paraelectric phase transition, identified by T_{FP}, and the higher temperature peak represents the melting temperature, T_m.

The Curie temperature, T_{FP}, is not influenced by the presence of the ionic liquid in the polymer matrix (Fig. 3 and Table 1), the observed differences being within the experimental error.

On the other hand, the melting temperature decreases with the increase of the ionic liquid content in the polymer matrix due to a disruption of the crystalline phase caused by the weak interaction between the ionic liquid and the polar polymer chains for large amounts of ionic liquid, above 16wt. % and also due to the plasticization effect of IL [47]. The interaction between the ionic liquid and the polymer matrix improves proper material crystallization and also accelerates the segmental motion of the P (VDF-TrFE) polymer chains [48] as observed in Table 1 for the degree of crystallinity. The degree of crystallinity only decreases for large amounts of ionic liquid, above 16wt. % due to the Coulomb interaction between IL and the polymer chains that results in an increased number of crystallization nuclei and a better packing of molecular chains [46].

The AC impedance (Nyquist plot) for the solid polymer electrolytes is shown in Fig. 4. This figure illustrates the mobility of ions due to charge transfer and diffusion processes. Typically, the Nyquist plot is described by three distinct parts: a semicircle located at the high-frequency range that corresponds to the charge transfer process, a straight line for

lower frequencies that is related to the diffusion process and the transition between these phenomena [49,50].

a)

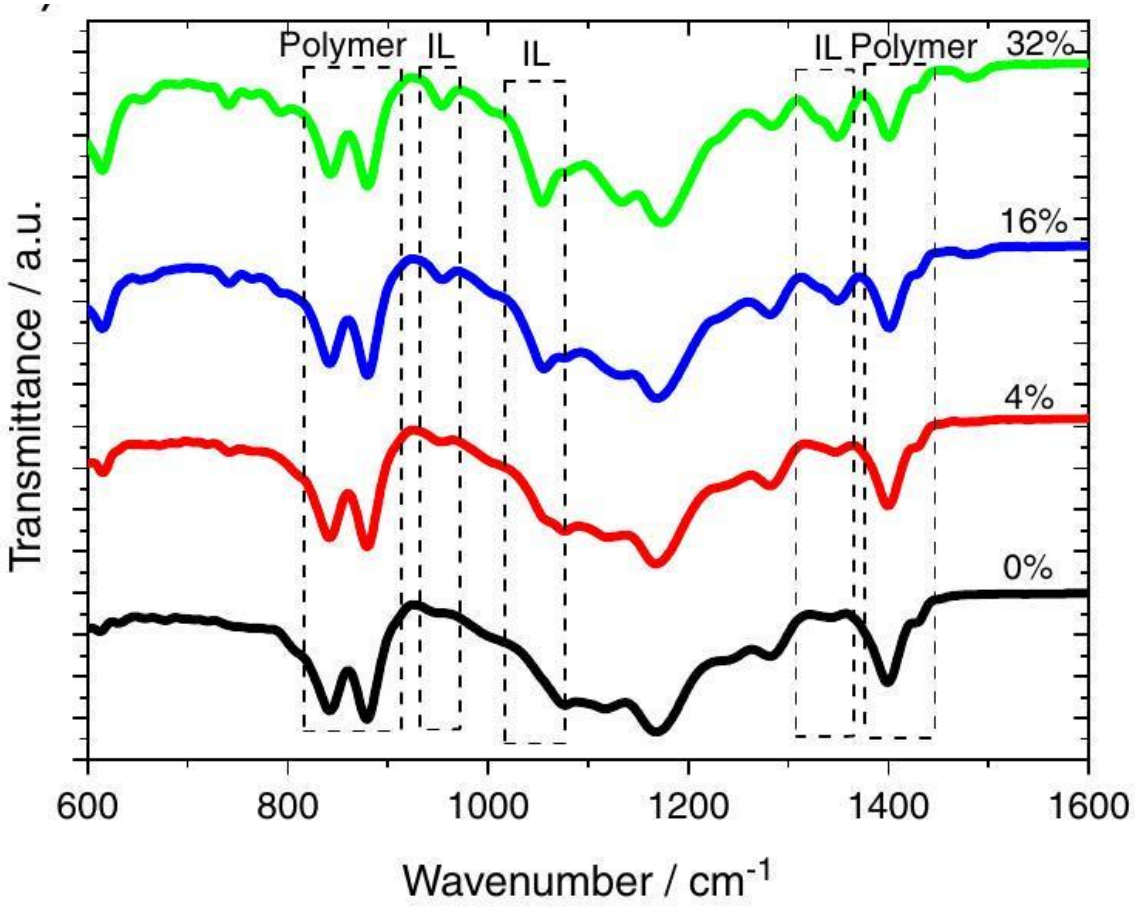

b)

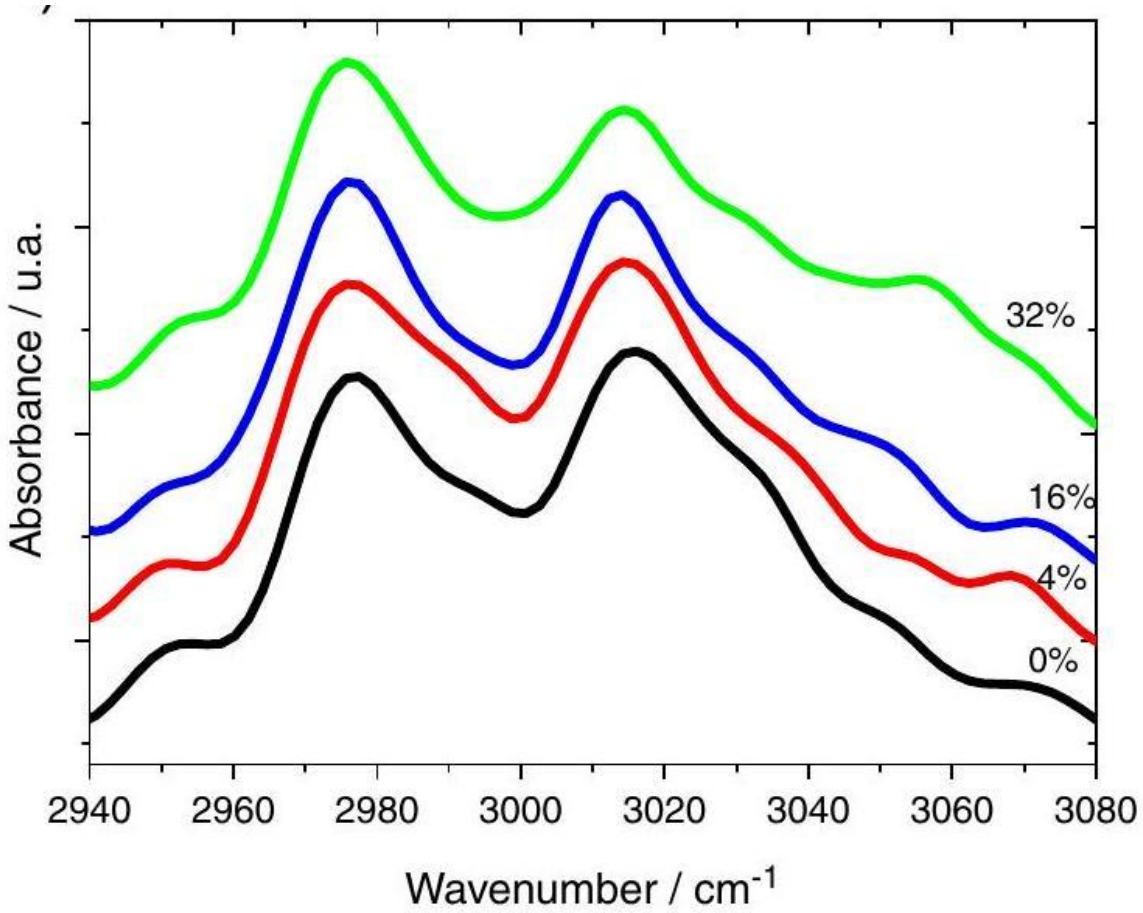

Fig. 2. FTIR spectra of the P(VDF-TrFE) and the SPEs with different IL contents: a) 6001600 cm^{-1} and b) in absorbance mode of the C-H mode region at 2940-3080 cm^{-1}.

It is observed a semicircle associated to the ionic resistance of the samples in the high frequency range which increases with the increase of the ionic liquid content up to 4wt. %, as shown in Fig. 4a and b. Fig. 4a does not show a very noticeable semicircle due to the high ionic resistance of P(VDF – TrFE) and the absence of ionic liquid.

For an ionic liquid content above 4wt. % (Fig. 4c and d) just the straight line is detected due to the quantity and migration of charges and/or the surface in-homogeneity of the electrodes [51].

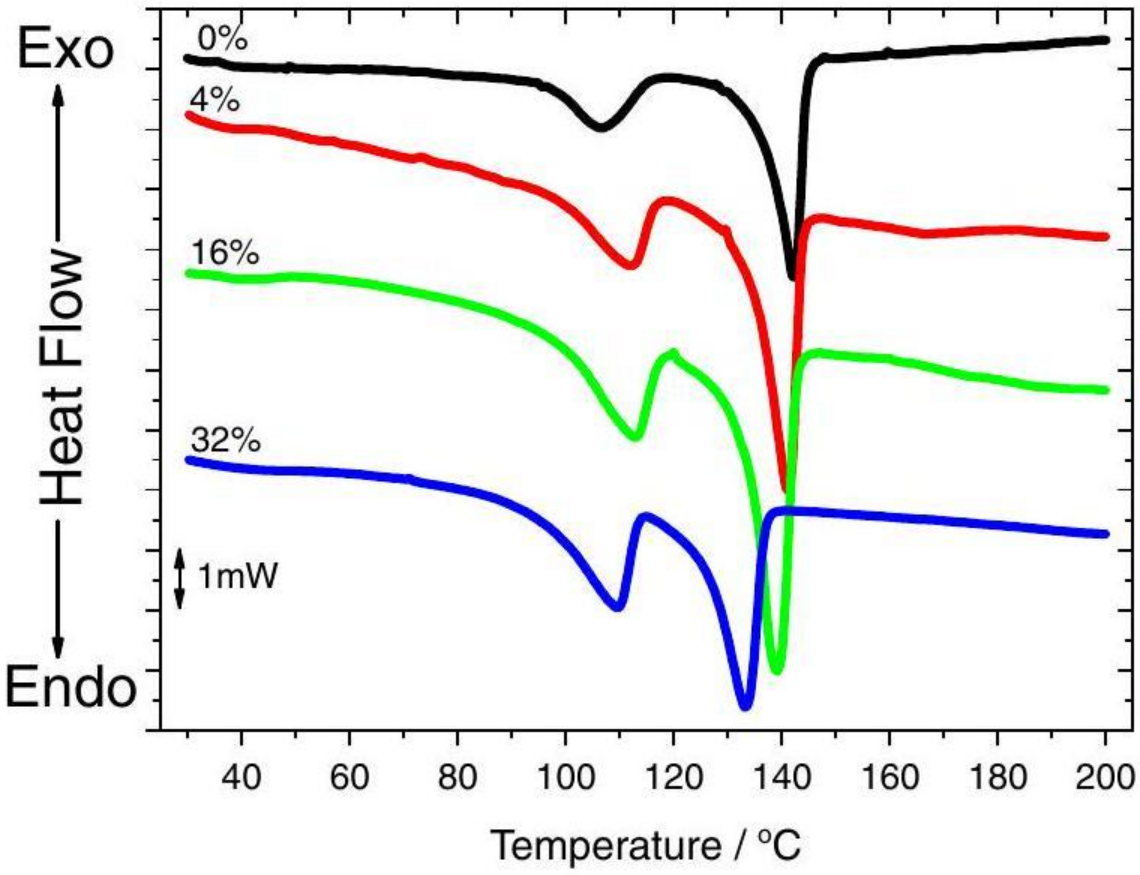

Fig. 3. DSC thermograms of the P(VDF-TrFE) membranes with different IL contents.

For the polymer electrolyte with 4wt.% ionic liquid content (Fig. 4b), at temperatures above 50°C (results not shown), a decrease of the semicircle is detected due to the increase of the ionic resistance of the ionic liquid.

The straight line that is observed in Fig. 4c and d is attributed to Warburg impedance in the diffusion process [30].

The equivalent circuit for analyzing the reaction mechanisms and kinetic parameters present in the solid polymer electrolytes [52] is, in the present case, a modified Randles circuit [53,54] (Fig. 5), where R_1, represents the electrolyte between the working and reference electrodes in parallel with a capacitance representing the interface between solid polymer membrane with ionic liquid and electrodes, CPE_1 (that describe the behavior of nonideal capacitors [55]).

The charge-transfer resistance (R_2) in parallel of Warburg impedance (Z_w) reflects the influence of the mass transport of electroactive species on the total impedance of the electrochemical cell [54,56]. The double-layer capacitance (CPE_2) represents the capacitance of the film.

Fig. 6 shows the simulated Nyquist plot by the equivalent circuit described in Fig. 5 for 4wt.% and 32wt.%, respectively.

The solid line in Fig. 6 indicates the good agreement between the experimental data and the equivalent circuit.

In Fig. 6 the two processes are observed: the charge transfer and the diffusion of the ionics species. It was verified that these processes depend on the ionic liquid content and that for larger amounts of ionic liquid (above 4wt.%) the diffusion becomes the main process characterizing the SPE.

Table 2 shows the parameters obtained by the fitting with the equivalent circuit for all SPE membranes. The parameter n_2 shows a high value close to 1 for all the membranes, indicating a capacitive behavior.

The capacitance C_1 increases and the resistance values (R_1, R_2) decrease with increasing ionic liquid content in the polymeric matrix. The fact of the increasing capacitance is related with the electric double layer capacitor effect using ionic liquid and the decrease in resistance is ascribed to the release and mobility of the ionic charges through of ionic liquid within the polymeric matrix. The value of the Warburg impedance element (Z_w) is elevated and represents the diffusion process of ions at the electrode-electrolyte interfacial region. The value of this element increases with the ionic liquid content until the ionic diffusion within the solid polymer membrane is fast enough (Fig. 4c and d).

To complement the results from the Nyquist plot (Fig. 4), Fig. 7 shows the Bode plot (impedance and phase as a function of frequency) for all the SPEs.

Fig. 7a illustrates the impedance modulus as a function of frequency for all membranes at 50°C. Independently of the ionic liquid content, the impedance modulus decreases with the increase of the frequency due to the localized dynamics of the ion mobility. For a given frequency, e.g. 1 kHz , it is observed that the impedance modulus decreases with increasing ionic liquid content up to 16wt.% due to the higher carrier number in the polymer electrolyte (Fig. 8). For 32 wt.%, at low frequency, the impedance modulus increases probability due to the formation of multiple ions (aggregates, result of the ion-ion interactions), that reduce the ionic mobility.

The phase angle as a function of frequency for all the SPEs at 50°C is shown in Fig. 7b. It can be seen that the phase angle values decrease with increasing ionic liquid content and it follows the order 0wt.% > 32wt.% > 16wt.% > 4wt.% at 1 kHz . This behavior is due to the polarization relaxation process existing in the SPEs that depends on the ionic liquid content [57]. At 1 kHz , the maximum phase angle occurs at 70° for 16wt.% and 32wt.%. Observing the Fig. 7b, the maximum of the phase angle is lower than 90°, the behavior being characterized by a constant phase element (CPE), which can be modeled as a capacitor with a distribution of relaxation times [58,59].

Fig. 8a shows the impedance modulus as a function of the ionic liquid content at three different temperatures (20°C, 50°C and 100°C). For 20°C, the impedance modulus decreases by increasing the ionic liquid content due to the higher number of charge carriers. With respect to

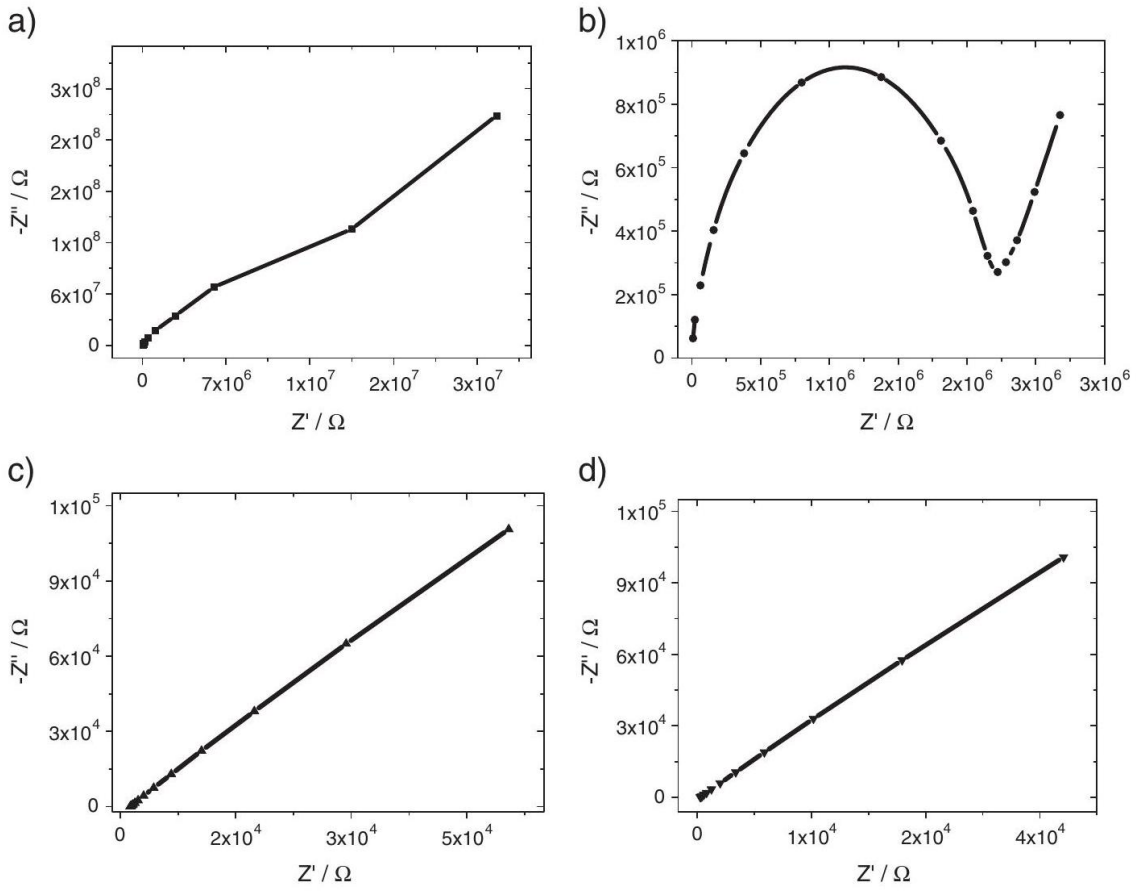

Fig. 4. Nyquist plot of the P(VDF − TrFE) composites at 50 °C with IL contents of a) 0wt. %, b)4wt. %, c)16wt. % and d) 32wt. %.

the temperatures of 50 and 100°C, the impedance modulus decreases until 16wt% and increases for polymer electrolyte membrane with 32wt. %. This may be due to the high salt concentration that enhances the formation of ion pairs and aggregates [60].

At room temperature (Fig. 8b), the maximum value of the ionic conductivity (Eq. (2)) is 1.7×10^{-5} S · cm^{-1} for 32wt%. The ionic conductivity increases with the increase of the ionic liquid content because the dissociation and ion transport of the ionic liquid results in higher carrier numbers in the polymer matrix. Moreover, the higher amount of ionic liquid present in the polymer matrix weakens the interaction among the polymer chains and accelerates the dissociation of the ion transport from polymer chain motion that depends on the temperature, as shown in Figs. 8a and 7 [47].

The temperature dependence of the ionic conductivity calculated after Eq. (2) for all the solid polymer electrolytes is shown in Fig. 9. It is observed that the addition of the ionic liquid increases the ionic conductivity of all the membranes in comparison to the pristine polymer in the entire temperature range under consideration, as shown in Fig. 9.

For higher ionic liquid content (above 4wt%), it is detected a stabilization of the ionic conductivity value over the temperature range,

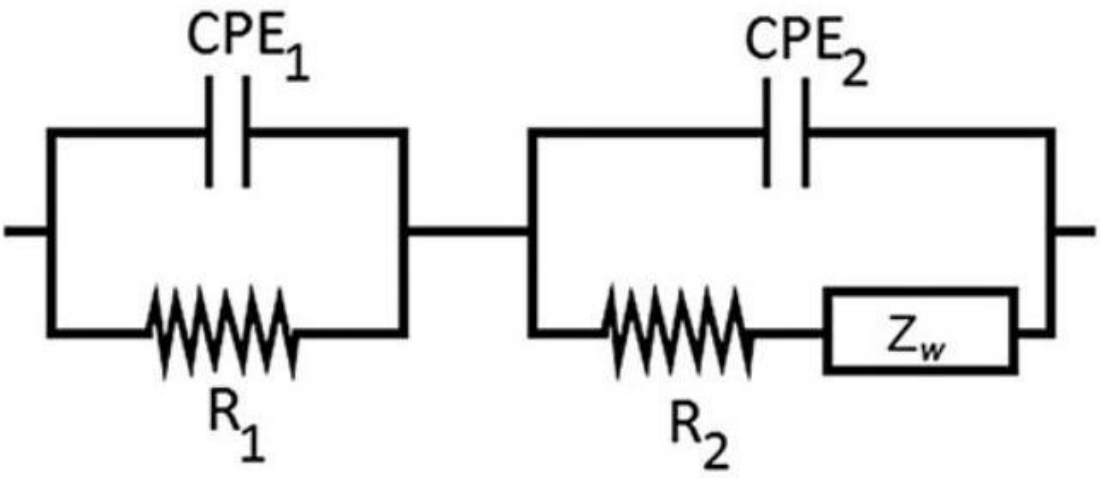

Fig. 5. Scheme representation of the equivalent circuit model used for the P (VDF-TrFE)/ ionic liquid SPEs.

indicating that the membranes do not depend as strongly on temperature as the pristine polymer, being more suitable for battery separators.

The ionic conductivity of the polymer electrolyte with ionic liquid is due to the conduction of both cation and anion moieties [61,62].

The temperature behavior of the ionic conductivity of the polymer electrolyte (Fig. 9) membranes follows the Arrhenius equation in the measured temperature range:

$$\sigma = \sigma_0 \exp\left(\frac{-E_a}{RT}\right) \quad (3)$$

where σ is the ionic conductivity, σ_0, E_a, R and T are the pre-exponential factor, the apparent activation energy for ion transport, the gas constant ($8.314\ \mathrm{J/mol \cdot K}$) and the temperature, respectively.

The obtained parameters after fitting the data from Fig. 9 are shown in Table 3. It is observed that both parameters σ_0 and E_a decrease with the increase of the ionic liquid content.

The E_a values decrease considerably with the addition of ionic liquid due to enhancement of segmental motion of the polymer chains and increase of ionic mobility.

The pre-exponential factor decreases with the increase of ionic liquid content as a result of the relative increase of the ionic conductivity, ionic liquid containing phase.

For battery separator applications, it is necessary to investigate the electrochemical operation window within the operation voltage of the battery applications [34].

The electrochemical window of the solid polymer electrolytes with ILs was determined by cyclic voltammetry over the potential range -2.0 V to 6.0 V through the following configuration: gold microelectrode/SPE/lithium disk electrode and is represented in Fig. 10 for the different SPEs.

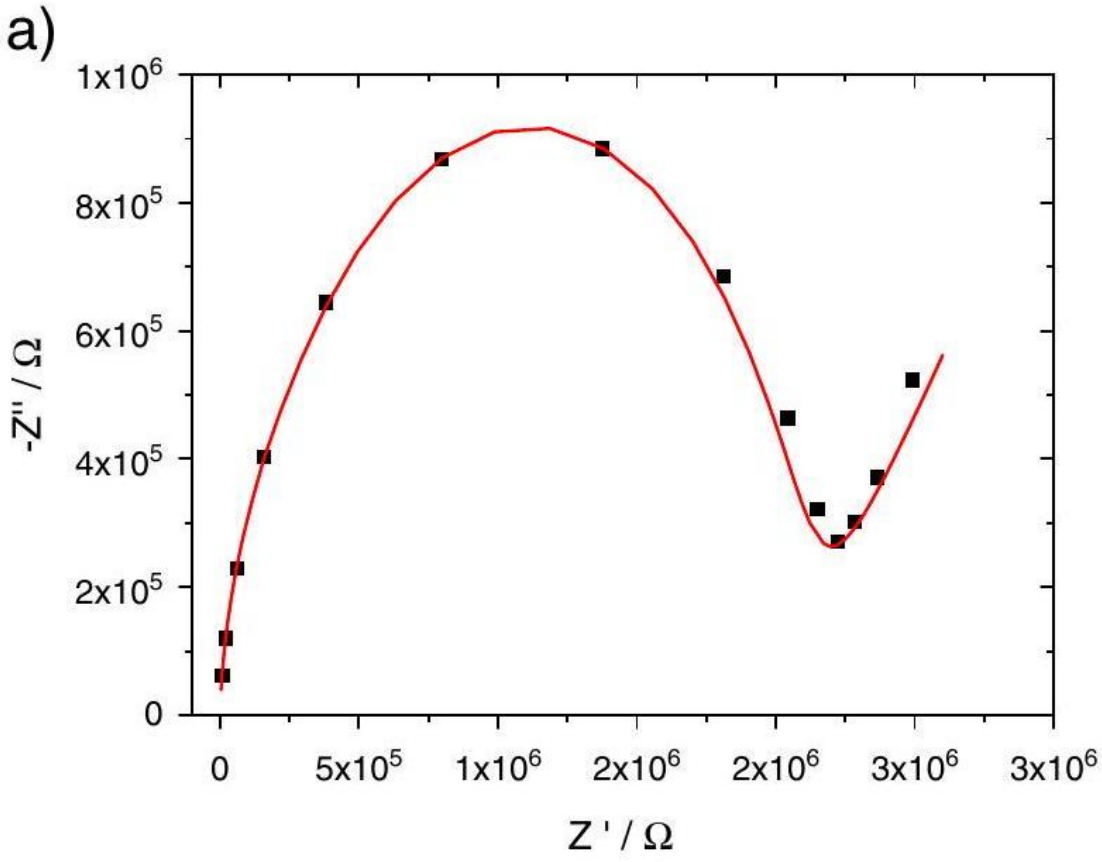
a)
1x10^6
8x10^5
6x10^5
4x10^5
2x10^5
0
-Z'' / Ω
0
5x10^5
1x10^6
2x10^6
2x10^6
3x10^6
3x10^6
Z ' / Ω

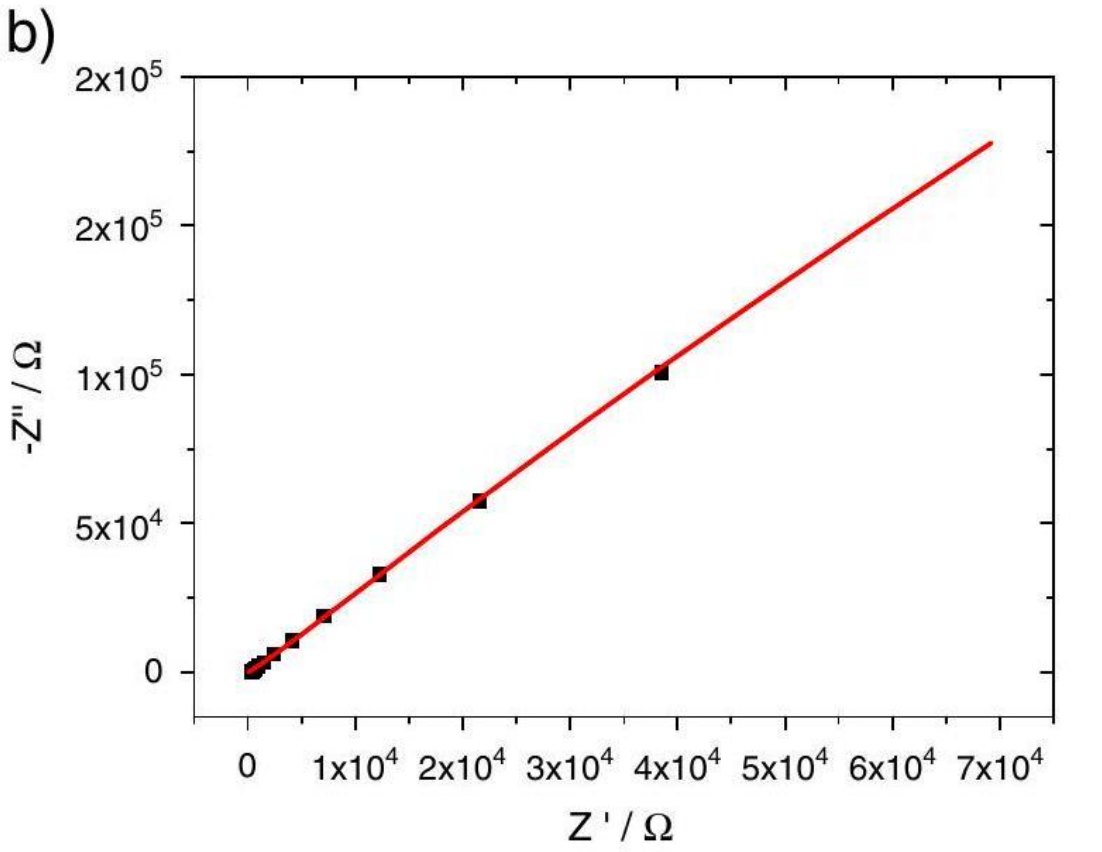
b)
2x10^5
2x10^5
1x10^5
5x10^4
0
-Z'' / Ω
0
1x10^4
2x10^4
3x10^4
4x10^4
5x10^4
6x10^4
7x10^4
Z ' / Ω

Fig. 6. Nyquist plot for P(VDF – TrFE) with $[N_1 1_1 1_2(OH)][NTf_2]$ and the corresponding fitting with equivalent circuit for: a) 4wt. % and b) 32wt. %.

From the voltammograms, the diffusion coefficients of the electroactive species (D) were also calculated according to the Randles-Sevcik equation [63]:

$$i_p = (2.69 \times 10^5) n^{3/2} A D^{1/2} v^{1/2} C_0 \quad (4)$$

where i_p is the oxidative peak current, n is the number of ionic charges involved in the electrode reaction, A is the electrode area, v is the potential scan rate and C_0 is the concentration of the electroactive species.

For the same scanning rate (0.5 V/s, Fig. 10a one anodic potential higher than 4.0 V is verified that depends on the ionic liquid content.

In Fig. 10b it is observed the voltammogram of solid polymer membrane with 16wt. % of ionic liquid at different scanning rates at

Table 2
Values obtained for the different parameters fitted with the equivalent circuit represented in Fig. 5.

	Samples		
Parameters	4wt%	16wt. %	32wt. %
$R_1(\Omega)$	1.1×10^6	7×10^{-12}	3.7×10^{-10}
$R_2(\Omega)$	1.0×10^6	1341	629
$Z_w(\Omega)s^{-0.5})$	2.3×10^6	1.9×10^6	4.4×10^6
$C_1(F)$	3.1×10^{-10}	3.2×10^{-8}	0.0005
n_1	0.99	0.59	0.10
$C_2(F)$	2.2×10^{-10}	1.2×10^{-6}	3.9×10^{-7}
n_2	0.92	0.77	0.81

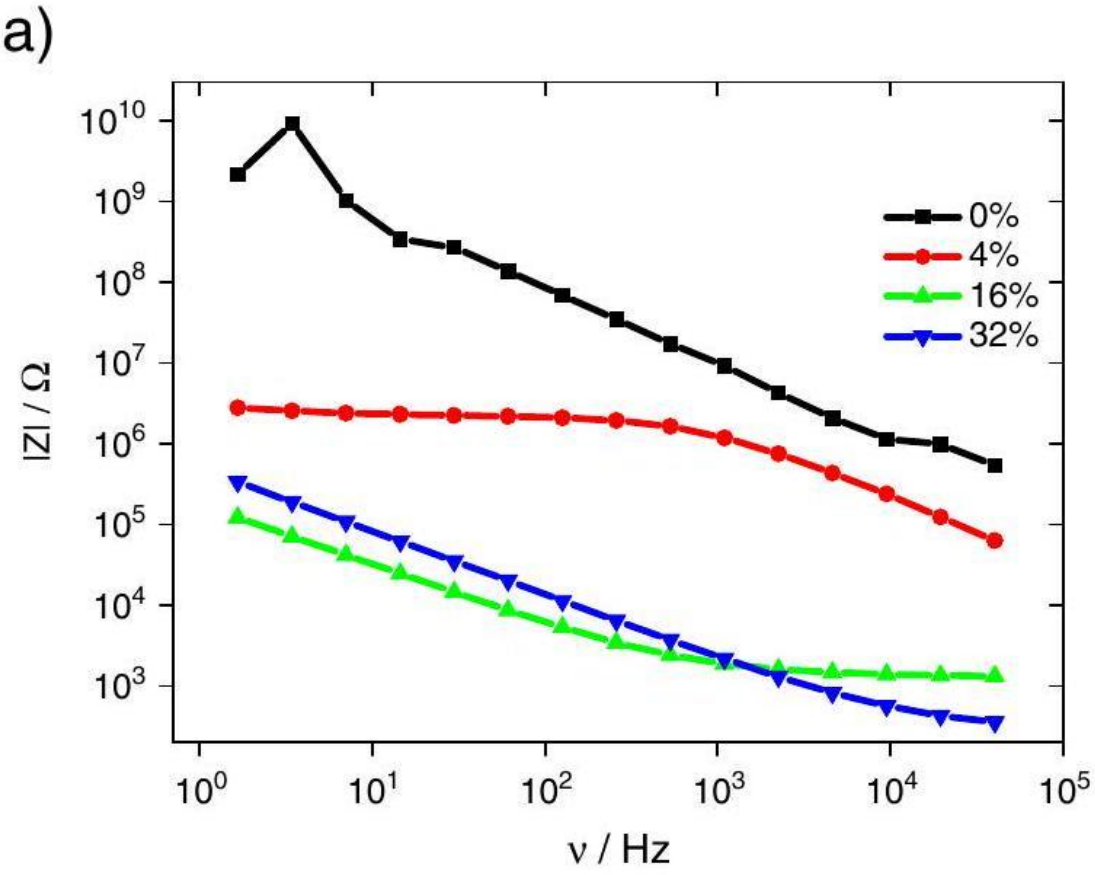
a)
|Z| / Ω
10^{10}
10^{9}
10^{8}
10^{7}
10^{6}
10^{5}
10^{4}
10^{3}
0%
4%
16%
32%
10^{0}
10^{1}
10^{2}
10^{3}
10^{4}
10^{5}
ν / Hz

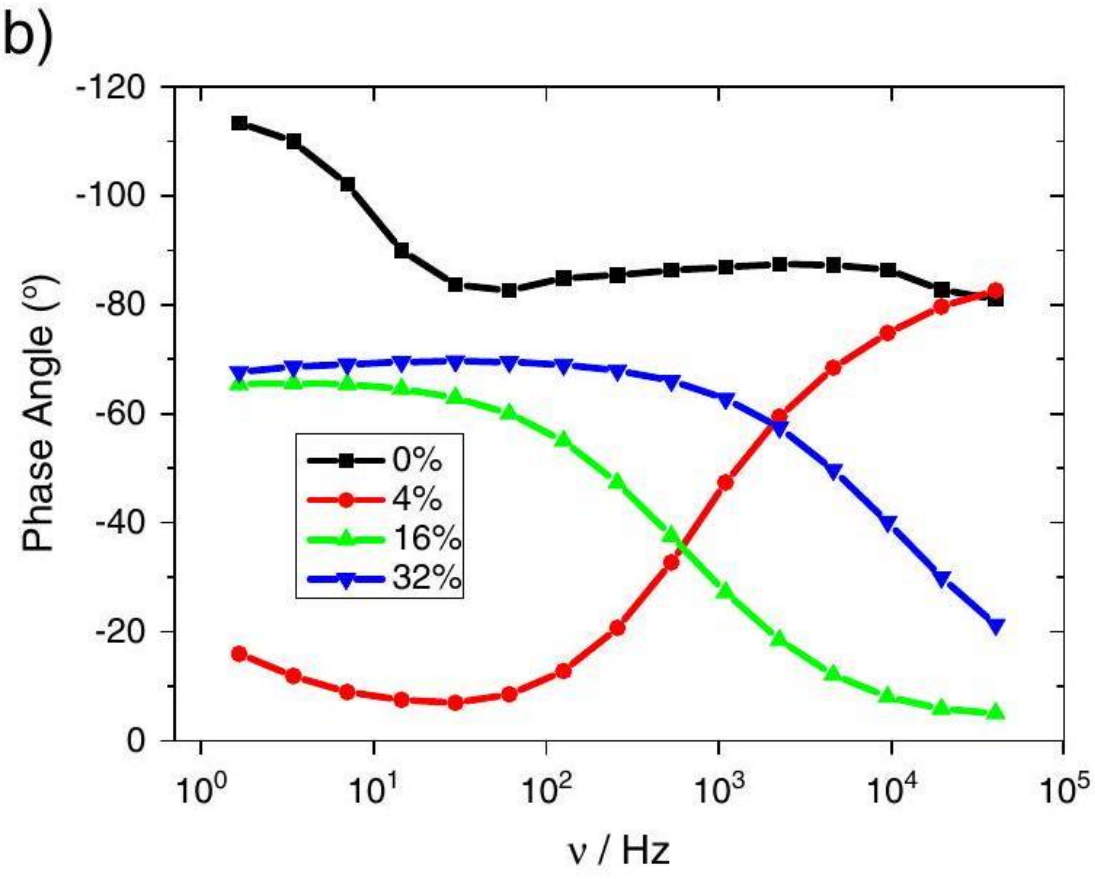
b)
Phase Angle (°)
-120
-100
-80
-60
-40
-20
0
0%
4%
16%
32%
10^{0}
10^{1}
10^{2}
10^{3}
10^{4}
10^{5}
ν / Hz

Fig. 7. a-b) Bode diagram of the $P(VDF-TrFE)/IL$ composites at 50°C. room temperature. It exhibits good electrochemical stability independently of scanning rate, with anodic potentials higher than 4.0 V and oxidation peak around 0.0 V . The anodic current onset may be associated with the decomposition of the polymer electrolyte. Increase of potential sweeping rate, shifts the cathodic peak potential in the negative direction.

The cathodic current onset observed at about 0.0 V may also correspond to the electrochemical deposition of lithium [34].

It is observed the presence of small peaks between 1.0 to -2.0 V (Fig. 10a for 32wt. %). Previously, the peaks in this region have been ascribed to reduction of low level of water present in polymer electrolytes or oxygen impurities. Analogous behavior has been observed for other systems based on PEO and lithium salt [34,64].

The voltammogram of all the solid polymer membranes (Fig. 10a) is correlated to the different ionic liquid content as verified through the diffusion coefficient calculated from Eq. (4). The diffusion coefficients of all the solid polymer membranes are in the order of 7.5×10^{-5} cm^2/s for the 16wt. % and 1.2×10^{-4} cm^2/s for the 32wt. %.

Through the diffusion coefficient and the electrochemical potential windows range determined for these membranes was shown that these solid polymer electrolyte are adequate and can be useful for energy storage applications.

Conclusions

Solid polymer electrolytes containing ionic liquid up to 32wt. % in a poly(vinylidene fluoride-trifluoroethylene) matrix were prepared by solvent-cast method. The ionic liquid was N,N,N-

a)

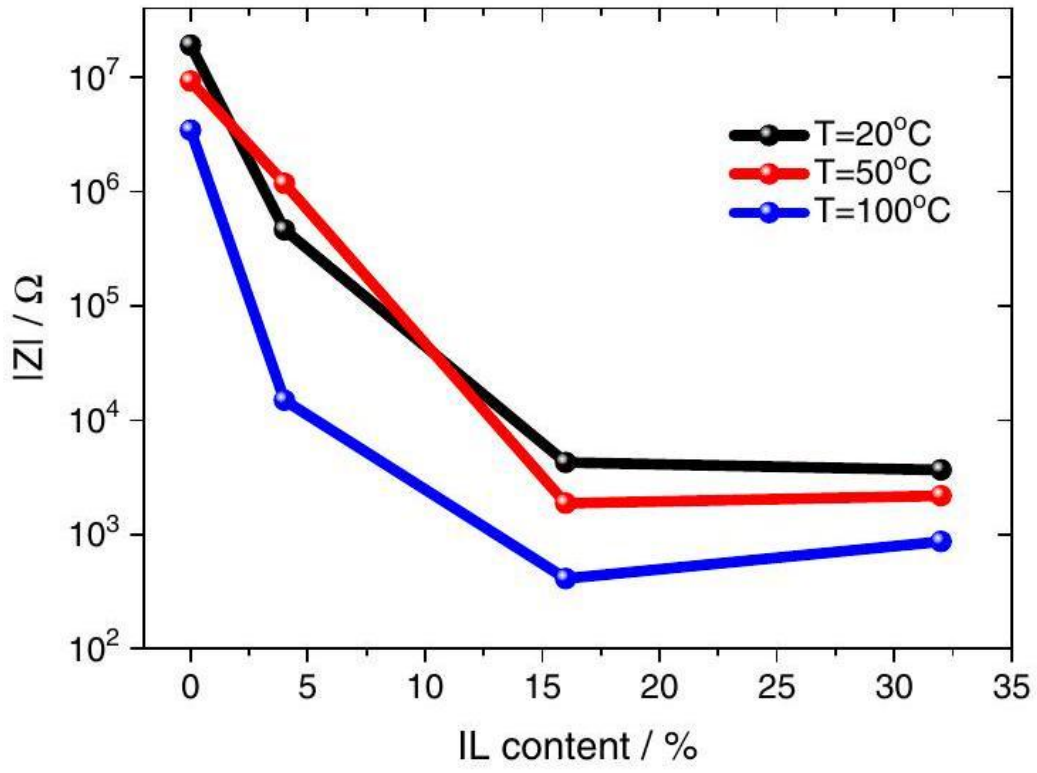

b)

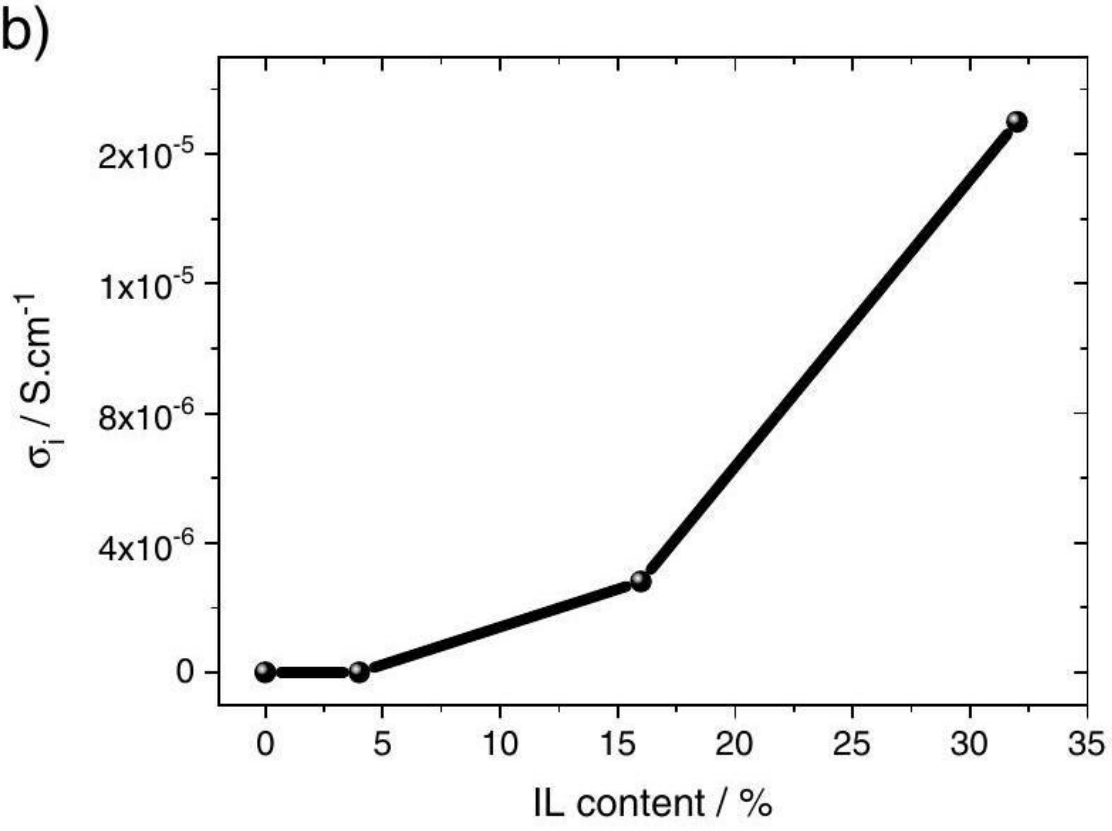

Fig. 8. a) Impedance modulus of the $P(VDF-TrFE)/IL$ composites at different temperatures and b) ionic conductivity calculated from Eq. (2) at room temperature for different IL contents. trimethyl-N-(2-hydroxyethyl)ammonium bis(trifluoromethylsulfonyl) imide, $[N_{1\,1\,1\,2}(OH)][NTf_2]$.

The morphology of the membranes observed through the SEM images depends on the ionic liquid content. The pore size increases and the spherulite size decreases with the increase of the ionic liquid content.

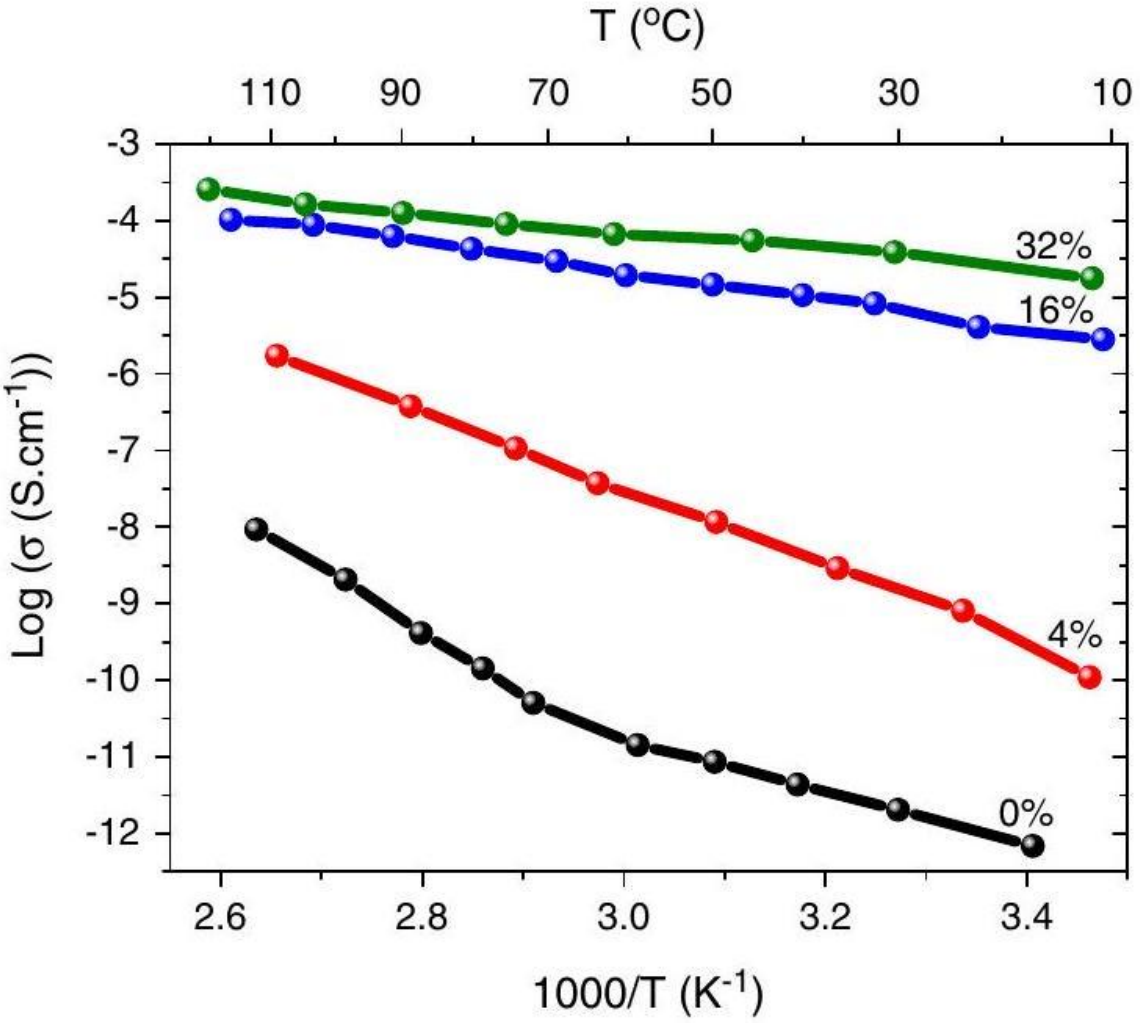

Fig. 9. Log σ as a function of 1000/T for P (VDF-TrFE)/IL composites with different IL contents.

Table 3
σ_0 and E_a for SPEs with different ionic liquid contents determined from the fitting of the Arrhenius equation to the data shown in Fig. 9.

Samples	$\sigma_0(Scm^{-1})$	$E_a(kJ/mol)$

0wt. %	2.3×10^3	43.90
4wt. %	2.2×10^3	42.20
16wt. %	2.64×10^0	15.60
32wt. %	6.1×10^{-1}	10.14

The polymer matrix crystallizes in the polar phase and this fact is independent of the inclusion of ionic liquid. The degree of crystallinity decreases to 17% for the 32wt% ionic liquid content membrane. The ionic conductivity increases and is stable in the temperature range from 25°C to 110°C, being the maximum room temperature ionic conductivity 1.7×10^{-5} S $\cdot$ cm^{-1} for the 32wt. %IL content sample. The equivalent circuit of these membranes is the Randles modified circuit.

The electrochemical stability evaluated by cyclic voltammetry reveals a stable operation window between -2.0 and 4.0 V . The diffusion coefficient determined for these membranes has shown that 1.2×10^{-4} cm^2/s for the 32wt. %. The results show that the prepared solid polymer electrolyte membranes have adequate morphological, thermal and electrochemical properties for energy storage applications.

Acknowledgments

This work was supported by FEDER through the COMPETE Program and by the Portuguese Foundation for Science and Technology (FCT) in

a)

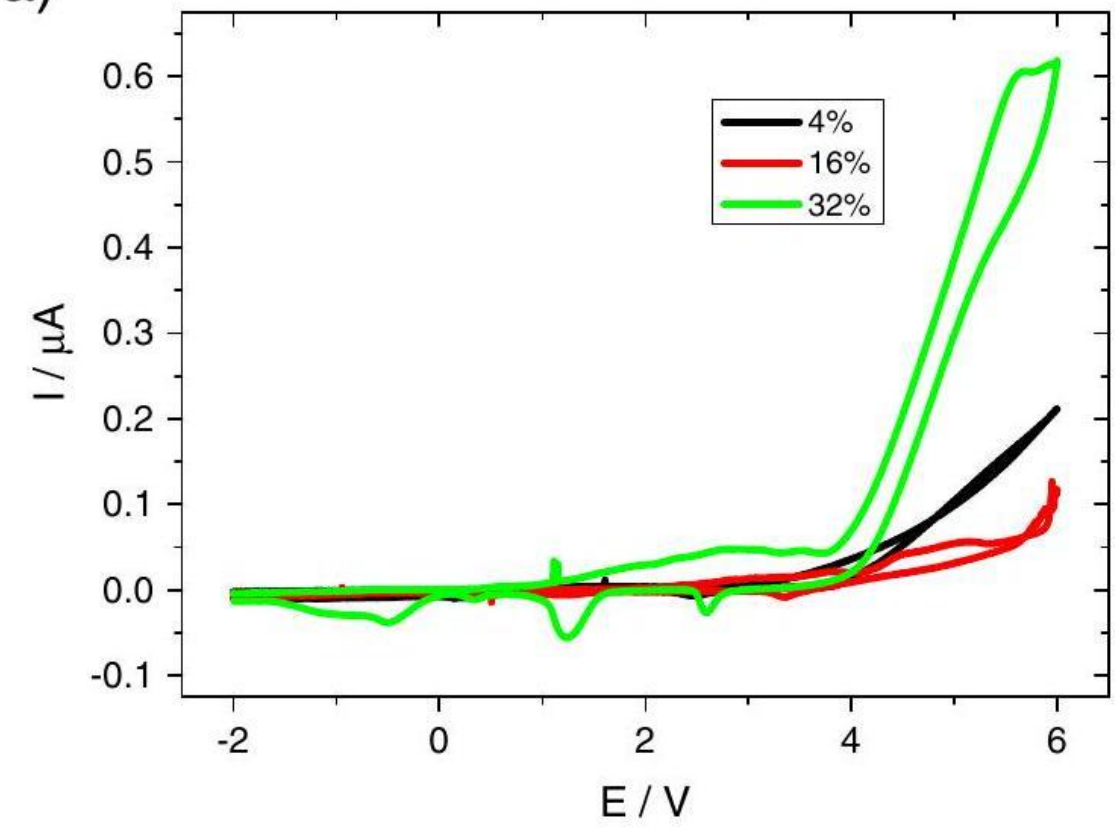
4%
16%
32%
I / µA
E / V
0.6
0.5
0.4
0.3
0.2
0.1
0.0
-0.1
-2
0
2
4
6

b)

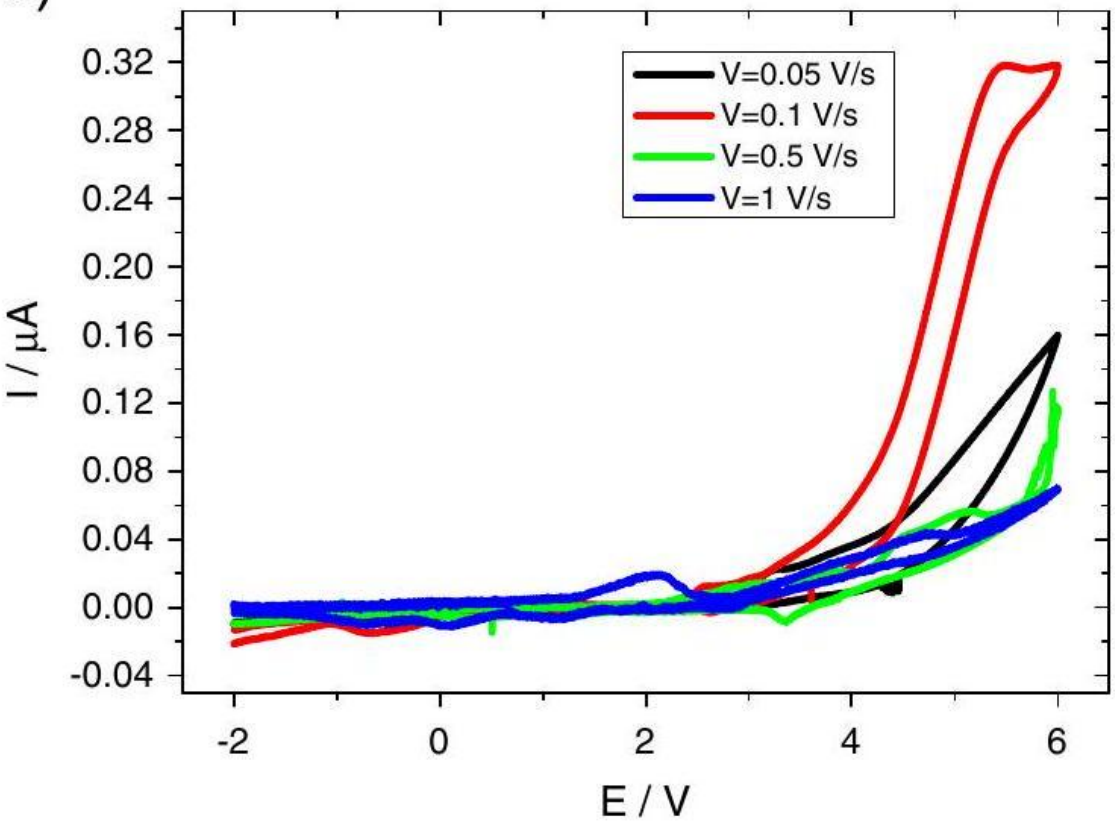
V=0.05 V/s
V=0.1 V/s
V=0.5 V/s
V=1 V/s
I / µA
E / V
0.32
0.28
0.24
0.20
0.16
0.12
0.08
0.04
0.00
-0.04
-2
0
2
4
6

Fig. 10. a) Voltammogram of P(VDF – TrFE)/IL composites at 0.5 V/s; b) voltammogram of P(VDF-TrFE)/IL composites with 16wt.% of IL at different scanning rates.

the framework of the Strategic Project PEST-C/FIS/UI607/2011, PEST-C/QUI/UI0686/2011, PEST-OE/EQB/LA0004/2011, and grants SFRH/BD/ 68499/2010 (C.M.C.) and SRFH/BD/90366/2012 (R.L.). The authors also thank funding from the "Matepro - Optimizing Materials and Processes", ref. "NORTE-07-0124-FEDER-000037", co-funded by the "Programa Operacional Regional do Norte" (ON. 2 - O Novo Norte), under the "Quadro de Referência Estratégico Nacional" (QREN), through the "Fundo Europeu de Desenvolvimento Regional" (FEDER).

The authors thank Solvay for kindly supplying the high quality materials.

References

[1] J.M. Tarascon, M. Armand, Nature 414 (6861) (2001) 359.
[2] E. Quartarone, P. Mustarelli, Chem. Soc. Rev. 40 (5) (2011) 2525.
[3] P.V. Wright, Electrochim. Acta 43 (10-11) (1998) 1137.
[4] M. Armand, Solid State Ionics 69 (3-4) (1994) 309.
[5] M.J. Smith, M.M. Silva, S. Cerqueira, J.R. MacCallum, Solid State Ionics 140 (3-4) (2001) 345.
[6] D. Benrabah, J.Y. Sanchez, M. Armand, Electrochim. Acta 37 (9) (1992) 1737.
[7] K. Scott, W. Taama, J. Cruickshank, J. Power Sources 65 (1-2) (1997) 159.
[8] G. Maggio, V. Recupero, L. Pino, J. Power Sources 101 (2) (2001) 275.
[9] P. Arora, Z. Zhang, Chem. Rev. 104 (10) (2004) 4419.
[10] P. Novák, K. Müller, K.S.V. Santhanam, O. Haas, Chem. Rev. 97 (1) (1997) 207.
[11] P. Gómez-Romero, C. Sanchez, Functional Hybrid Materials, Wiley, 2006.
[12] D. Ravaine, A. Seminel, Y. Charbouillot, M. Vincens, J. Non-Cryst. Solids 82 (1-3) (1986) 210.
[13] M. Popall, M. Andrei, J. Kappel, J. Kron, K. Olma, B. Olsowski, Electrochim. Acta 43 (10-11) (1998) 1155.
[14] P. Judeinstein, J. Titman, M. Stamm, H. Schmidt, Chem. Mater. 6 (2) (1994) 127.
[15] K. Dahmouche, M. Atik, N. Mello, T. Bonagamba, H. Panepucci, M. Aegerter, P. Judeinstein, J. Sol-gel, Sci. Technol. 8 (1-3) (1997) 711.
[16] F.M. Gray, Solid Polymer Electrolytes: Fundamentals and Technological Applications, Wiley, 1991.
[17] C.M. Costa, M.M. Silva, S. Lanceros-Mendez, RSC Adv. (2013), http://dx.doi.org/10.1039/C3RA40732B.
[18] J.R. Kim, S.W. Choi, S.M. Jo, W.S. Lee, B.C. Kim, Electrochim. Acta 50 (1) (2004) 69.
[19] C.M. Costa, L.C. Rodrigues, V. Sencadas, M.M. Silva, S. Lanceros-Méndez, Solid State Ionics 217 (2012) 19.
[20] C.M. Costa, L.C. Rodrigues, V. Sencadas, M.M. Silva, J.G. Rocha, S. Lanceros-Méndez, J. Membr. Sci. 407-408 (2012) 193.
[21] I. Renard, H. Li, B.T. Marsan, Electrochim. Acta 48 (7) (2003) 831.
[22] Y.-S. Ye, J. Rick, B.-J. Hwang, J. Mater. Chem. A 1 (8) (2013) 2719.
[23] M. Armand, F. Endres, D.R. MacFarlane, H. Ohno, B. Scrosati, Nat. Mater. 8 (8) (2009) 621.
[24] K.N. Marsh, J.A. Boxall, R. Lichtenthaler, Fluid Phase Equilib. 219 (1) (2004) 93.
[25] M.J. Earle, J.M.S.S. Esperanca, M.A. Gilea, J.N. Canongia Lopes, L.P.N. Rebelo, J.W. Magee, K.R. Seddon, J.A. Widegren, Nature 439 (7078) (2006) 831.
[26] M. Smiglak, W.M. Reichert, J.D. Holbrey, J.S. Wilkes, L. Sun, J.S. Thrasher, K.

Kirichenko, S. Singh, A.R. Katritzky, R.D. Rogers, Chem. Commun. (24) (2006) 2554.
[27] K.J. Baranyai, G.B. Deacon, D.R. MacFarlane, J.M. Pringle, J.L. Scott, Aust. J. Chem. 57 (2) (2004) 145.
[28] F. Endres, Z. Phys. Chem. 218 (2-2004) (2004) 255.
[29] J.D. Holbrey, K.R. Seddon, Clean Prod. Processes 1 (4) (1999) 223.
[30] M. Egashira, H. Todo, N. Yoshimoto, M. Morita, J. Power Sources 178 (2) (2008) 729.
[31] H. Ohno, Electrochemical Aspects of Ionic Liquids, Wiley, 2011.
[32] E.F. Borra, O. Seddiki, R. Angel, D. Eisenstein, P. Hickson, K.R. Seddon, S.P. Worden, Nature 447 (7147) (2007) 979.
[33] A.J.L. Costa, M.R.C. Soromenho, K. Shimizu, I.M. Marrucho, J.M.S.S. Esperança, J.N.C. Lopes, L.P.N. Rebelo, ChemPhysChem 13 (7) (2012) 1902.
[34] H. Cheng, C. Zhu, B. Huang, M. Lu, Y. Yang, Electrochim. Acta 52 (19) (2007) 5789.
[35] S.-H. Yeon, K.-S. Kim, S. Choi, J.-H. Cha, H. Lee, J. Phys. Chem. B 109 (38) (2005) 17928.
[36] S.-H. Yeon, K.-S. Kim, S. Choi, J.-H. Cha, H. Lee, J. Oh, B.-B. Lee, Korean J. Chem. Eng. 23 (6) (2006) 940.
[37] J. Fuller, A.C. Breda, R.T. Carlin, J. Electroanal. Chem. 459 (1) (1998) 29.
[38] G.P. Pandey, S.A. Hashmi, J. Power Sources 187 (2) (2009) 627.
[39] C.M. Costa, V. Sencadas, J.G. Rocha, M.M. Silva, S. Lanceros-Méndez, J. Solid State Electrochem. 17 (3) (2013) 861.
[40] H.S. Nalwa, Ferroelectric Polymers: Chemistry, Physics, and Applications, Marcell Dekker, Incorporated, 1995.
[41] R.S. Porter, J. Polym. Sci.: Polym. Lett. Ed. 20 (11) (1982) 602.
[42] A. Ferreira, J. Silva, V. Sencadas, J.L.G. Ribelles, S. Lanceros-Méndez, Macromol. Mater. Eng. 295 (6) (2010) 523.
[43] A.A. Prabu, J.S. Lee, K.J. Kim, H.S. Lee, Vib. Spectrosc. 41 (1) (2006) 1.
[44] S. Wolf, C. Feldmann, Dalton Trans. 41 (27) (2012) 8455.
[45] P. Martins, A.C. Lopes, S. Lanceros-Méndez, Prog. Polym. Sci. (2013), http://dx.doi.org/ 10.1016/j.progpolymsci.2013.07.006.
[46] F. Wang, A. Lack, Z. Xie, P. Frubing, A. Taubert, R. Gerhard, Appl. Phys. Lett. 100 (6) (2012) 062903.
[47] Shalu, S.K. Chaurasia, R.K. Singh, S. Chandra, J. Phys. Chem. B 117 (3) (2012) 897.
[48] J. Jiang, D. Gao, Z. Li, G. Su, React. Funct. Polym. 66 (10) (2006) 1141.
[49] B.-Y. Chang, S.-M. Park, Annu. Rev. Anal. Chem. 3 (1) (2010) 207.
[50] M. Park, X. Zhang, M. Chung, G.B. Less, A.M. Sastry, J. Power Sources 195 (24) (2010) 7904.
[51] M. Marcinek, A. Bac, P. Lipka, A. Zalewska, G. Żukowska, R. Borkowska, W. Wieczorek, J. Phys. Chem. B 104 (47) (2000) 11088.
[52] D.A. Harrington, P. van den Driessche, Electrochim. Acta 56 (23) (2011) 8005.
[53] J. Hernández-Ferrer, A. Ansón-Casaos, M.T. Martínez, Electrochim. Acta 64 (2012) 1.
[54] C. Fernández-Sánchez, C.J. McNeil, K. Rawson, TrAC Trends Anal. Chem. 24 (1) (2005) 37.
[55] A. Lasia, in: B.E. Conway, J.O.M. Bockris, R. White (Eds.), Modern Aspects of Electrochemistry, Springer US, 2002, pp. 143-248.
[56] E. Barsoukov, J.R. Macdonald, Impedance Spectroscopy: Theory, Experiment, and Applications, Wiley, 2005.
[57] A. Triolo, O. Russina, C. Hardacre, M. Nieuwenhuyzen, M.A. Gonzalez, H. Grimm, J. Phys. Chem. B 109 (46) (2005) 22061.
[58] K. Cole, J. Chem. Phys. 9 (4) (1941) 341.
[59] I.D. Raistrick, Annu. Rev. Mater. Sci. 16 (1) (1986) 343.

[60] G.B. Appetecchi, W. Henderson, P. Villano, M. Berrettoni, S. Passerini, J. Electrochem. Soc. 148 (10) (2001) A1171.
[61] H. Tokuda, K. Hayamizu, K. Ishii, M.A.B.H. Susan, M. Watanabe, J. Phys. Chem. B 108 (42) (2004) 16593.
[62] H. Tokuda, K. Ishii, M.A.B.H. Susan, S. Tsuzuki, K. Hayamizu, M. Watanabe, J. Phys. Chem. B 110 (6) (2006) 2833.
[63] L.R.F.A.J. Bard, Electrochemical Methods, John Wiley & Sons, New York, 2001.
[64] D. Aurbach, M. Daroux, P. Faguy, E. Yeager, J. Electroanal. Chem. Interfacial Electrochem. 297 (1) (1991) 225.